



TITLE:

Single crystal growth of the metallic triangular-lattice antiferromagnet PdCrO₂

AUTHOR(S):

Takatsu, Hiroshi; Maeno, Yoshiteru

CITATION:

Takatsu, Hiroshi ...[et al]. Single crystal growth of the metallic triangular-lattice antiferromagnet PdCrO₂. Journal of Crystal Growth 2010, 312(23): 3461-3465

ISSUE DATE:

2010-11-15

URL:

<http://hdl.handle.net/2433/131816>

RIGHT:

© 2010 Elsevier B.V.; この論文は出版社版ではありません。引用の際には出版社版をご確認ご利用ください。; This is not the published version. Please cite only the published version.

Single crystal growth of the metallic triangular-lattice antiferromagnet PdCrO_2

Hiroshi Takatsu, Yoshiteru Maeno

Department of Physics, Graduate School of Science, Kyoto University, Kyoto 606-8502, Japan

Abstract

We report details of single crystal growth of the metallic triangular-lattice antiferromagnet PdCrO_2 consisting of layers of Pd triangles and Cr triangles stacking along the c axis. We used the NaCl flux method and obtained the crystals with the size as large as $2 \times 3.5 \times 0.3 \text{ mm}^3$. We confirmed that single crystals have the delafossite structure with the $R\bar{3}m$ symmetry. The electrical resistivity along the c axis and that in the ab plane exhibit metallic temperature dependence with the anisotropic ratio ρ_c/ρ_{ab} of over 300 at low temperatures. The residual resistivity of as small as $\rho_{0,ab} = 45 \text{ n}\Omega \text{ cm}$ and the residual resistivity ratio of over 100 indicate high quality of the crystals investigated. Nevertheless, there is no sign of superconductivity down to 0.3 K. These crystals are useful for the investigation of anisotropic magnetic and transport properties including the unconventional anomalous Hall effect (AHE).

Key words: A1. Low dimensional structures, A2. Single crystal growth, B1. Oxides, B2. Magnetic materials

PACS: 61.66.Fn, 72.15.Eb, 72.80.Ga, 75.30.Gw,

1. Introduction

Delafossites ABO_2 (A : noble-metal elements; B : transition-metal and rare-earth elements) crystallize in a layered structure consisting of alternating stacks of triangular lattices (TL) of monovalent A^{1+} ions and trivalent B^{3+} ions along the c axis (Fig. 1). Because of the simple TL structure, members with the magnetic ions at the B site are useful for the clarification of the unresolved issues of ideal TL magnets [1, 2, 3, 4]. In addition, by the choice of A site ions, the metallicity can be controlled. Insulating delafossites are actively investigated as the typical multiferroic materials. For examples, CuFeO_2 [5] and CuCrO_2 [6, 7] are known to exhibit strong coupling between the spiral magnetic ordering with the proper-screw type spin structure and the ferroelectric polarization. Metallic delafossites with frustrated spin structure are promising for the investigation of the unconventional anomalous Hall effect (UAHE), which emerges not from the conventional order parameter magnetization M but possibly from the multi-spin quantity “scalar spin chirality” [8].

Although most delafossites are insulators or semiconductors, there are several members of metallic delafossites, such as AgNiO_2 [9, 10], PdCoO_2 [11, 12], PtCoO_2 [13, 14], and PdCrO_2 [15]. Among them, only AgNiO_2 and PdCrO_2 are magnetic metals. In particular, since metallic and magnetic origins are well separated in PdCrO_2 , this compound should provide unique opportunities to study the interplay between the localized frustrated spins and conduction electrons including UAHE [16].

Preprint submitted to Journal of crystal growth

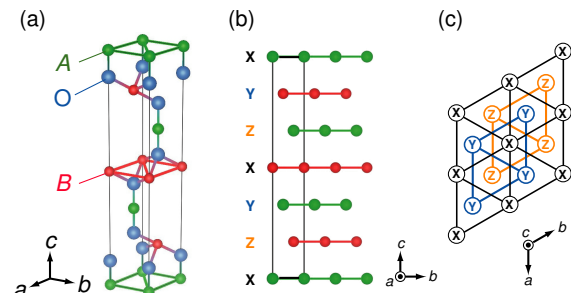


Figure 1: (a) Unit-cell crystal structure of delafossite ABO_2 . Both A and B ions form triangular lattices and stack along the c -axis in the sequence $B\text{-O-A-O-B}$. (b) Side view of the crystal structure. The oxygen ions above and below the A -site ions are not shown in this figure in order to focus on the layered structure of A and B atoms. The black lines indicate the unit cell. The symbols X, Y, and Z represent the stacking patterns of the layers. (c) Schematic drawing of the top view of the crystal structure. The definition of the symbols X, Y, and Z are the same as that in (b). These figures are generated by VESTA [17].

rated in PdCrO_2 , this compound should provide unique opportunities to study the interplay between the localized frustrated spins and conduction electrons including UAHE [16].

In order to clarify the mechanism of such unconventional transport properties, determinations of the Fermi surfaces and the detailed magnetic structure are neces-

August 17, 2010

sary. For these measurements, availability of the high-quality single crystals is crucial. Here, we present the details of the growth of high-quality PdCrO_2 single crystals. To the best of our knowledge, this is the first report of the details of the single crystal growth of PdCrO_2 .

Previous studies on powder samples of PdCrO_2 have revealed that it exhibits an antiferromagnetic transition at $T_N = 37.5$ K forming a 120° spin structure [18, 15]. This Neel temperature is an order of magnitude lower than the Weiss temperature $\theta_W \approx -500$ K; the frustration parameter $f \equiv |\theta_W|/T_N$ is about 13, indicating a strong frustration among spins. Single crystals obtained in this study revealed isotropic magnetization above T_N consistent with the Heisenberg spins, while they clarified the emergence of anisotropy below T_N , indicating that the 120° spin structure is easy-axis type.

2. Crystal growth

Single crystals of PdCrO_2 were grown by a NaCl flux method. Polycrystalline PdCrO_2 used for the single crystal growth were prepared in two steps. In the first step, LiCrO_2 was prepared as a precursor by the solid-state reaction of the stoichiometric mixture of Li_2CO_3 (99.99%, Aldrich Chemical Co.) and Cr_2O_3 (99.99%, Rare Metallic Co. Ltd.) at 850°C in air in an alumina crucible for 24 hours. In the second step, PdCrO_2 powder was synthesized by the following metathetical reaction: $\text{Pd} + \text{PdCl}_2 + 2\text{LiCrO}_2 \rightarrow 2\text{PdCrO}_2 + 2\text{LiCl}$ [13, 15, 19]. For this step, Pd powder (99.99%, Furuuchi Chem. Co.) and PdCl_2 powder (99.999%, Aldrich Chemical Co.) were used. The mixture was ground in a mortar for 30–60 minutes, sealed in an evacuated quartz tube (100 mm \times ϕ 10 mm), heated to 790°C and kept at this temperature for 96 hours. The obtained product was washed with aqua regia and distilled water to remove LiCl, unreacted Pd, and other by-products.

Single crystals were grown from the mixture of polycrystals of PdCrO_2 and NaCl (99.99%, Rare Metallic Co. Ltd.) with a mass ratio of typically 1 : 10. We note here that the minimum mass ratio in which single crystals were formed was 1 : 4. The mixture was sealed in an evacuated quartz tube (130 mm \times ϕ 20 mm), heated to 880°C in 3.5 hours, and kept at this temperature for 24 hours. It was then cooled down to 800°C at the cooling rate of $0.25\text{--}0.5^\circ\text{C/h}$ and to 700°C at 1°C/h . We should note that the melting point of NaCl is 801°C at ambient pressure. After the slow cooling processes, the quartz tube was furnace-cooled down to room temperature. Single crystals were obtained with by-products

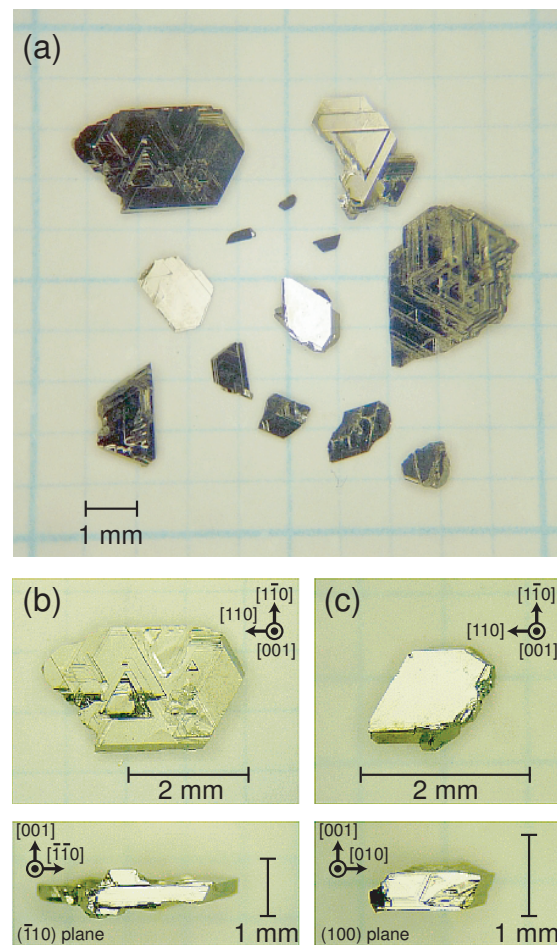


Figure 2: Optical microscope images of as-grown single crystals of PdCrO_2 .

such as Cr_2O_3 . In order to grow larger crystals, single crystals were added in the mixture as seeds. The largest crystal size obtained is about $2.0 \times 3.5 \times 0.3 \text{ mm}^3$ (see the microscope pictures in Fig. 2). We note here that single crystals of PdCrO_2 were not obtained either with PdCl_2 flux, Bi_2O_3 flux, or $\text{Bi}_2\text{O}_3\text{--B}_2\text{O}_3$ mixed flux. The starting PdCrO_2 polycrystals remained unreacted in PdCl_2 flux. They decomposed in Bi_2O_3 and $\text{Bi}_2\text{O}_3\text{--B}_2\text{O}_3$ fluxes but did not produce any crystals. We also note that attempts to grow the single crystals in air using Pt crucibles were not successful.

3. Characterization

Figure 3 represents the powder X-ray diffraction (XRD) spectra of polycrystalline and single-crystalline samples of PdCrO_2 , with the $\text{CuK}\alpha_1$ radiation. These

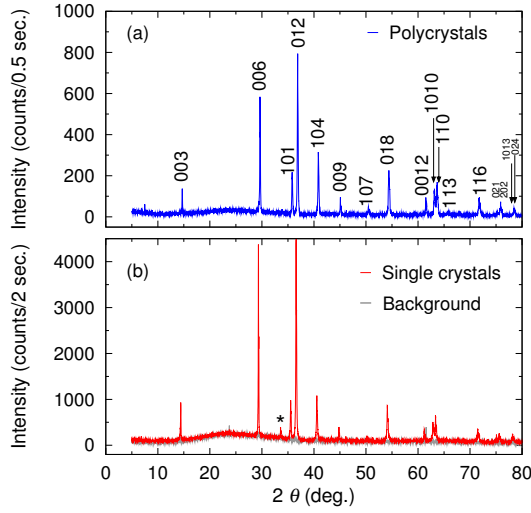


Figure 3: Powder XRD spectra of (a) polycrystalline samples and (b) crushed single-crystalline samples of PdCrO_2 at room temperature. The peak pattern can be labeled with the delafossite structure with $R\bar{3}m$ symmetry. The additional peak labeled with * for the single crystal spectrum at about $2\theta = 34^\circ$ originates from an impurity phase of Cr_2O_3 . It is well separated from the PdCrO_2 single crystals, but a small amount of powder Cr_2O_3 was inevitably picked up in the preparation for measurements.

two spectra exhibit the same patterns, yielding the lattice parameters of $a = b = 2.923 \text{ \AA}$, $c = 18.086 \text{ \AA}$ for both single crystals and polycrystals.

The X-ray Laue patterns for the (001) plane and (100) plane are presented in Figs. 4(a) and (b). Calculated patterns for these conditions shown in Figs. 4(c) and (d) are consistent with the measured patterns. The clear Laue spots guarantee high crystallinity of the crystals. Scanning electron microscope (SEM) images with the energy dispersive X-ray (EDX) analysis mapping are presented in Fig. 5. The EDX analyses confirmed the homogeneity of the crystals with the composition ratio of $\text{Pd}/\text{Cr} = 1.1 \pm 0.1$. Fig. 5 also indicates the Cr_2O_3 impurity phase localized on the left edge of the crystal.

Figure 6(a) represents the electrical resistivity along the c axis (ρ_c) and in the ab plane (ρ_{ab}) measured with both the ac and dc four-probe methods from 300 K to 0.32 K. Both ρ_c and ρ_{ab} exhibit metallic temperature dependence down to the lowest measurement temperatures with clear anomalies at T_N . The residual resistivities are $\rho_{0,c} = 16.5 \mu\Omega \text{ cm}$, $\rho_{0,ab} = 45 \text{ n}\Omega \text{ cm}$ (see the inset of Fig. 6). The residual resistivity ratio, $\text{RRR} \equiv \rho(295\text{K})/\rho(0.32\text{K})$, is estimated to be 104 for ρ_c and 200 for ρ_{ab} . By using the value of the Fermi wave number $k_F = 0.93 \text{ \AA}^{-1}$ [20] and the carrier den-

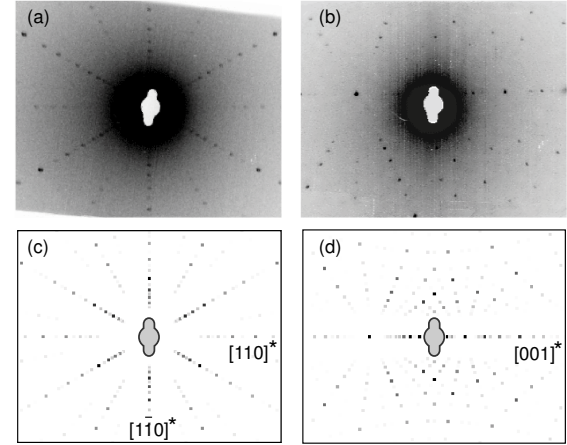


Figure 4: X-ray Laue patterns of (a) the (001) plane and (b) the (100) plane in back-scattered conditions. The photos exhibit clear spots that agree with the $R\bar{3}m$ symmetry. (c) and (d): the corresponding calculated patterns.

sity $n = 1.62 \times 10^{22} \text{ cm}^{-3}$ [21], the mean free path $l = (\hbar k_F / ne^2 \rho_0)$ in the ab plane is estimated to be as large as $l_{ab} \simeq 30 \mu\text{m}$. These large RRR and l guarantee high quality of the obtained crystals. The anisotropic ratio ρ_c/ρ_{ab} is over 190 in the whole measurement temperature range. The large anisotropy of the resistivity is consistent with the expectation that the metallic conductivity mainly originates from the Pd layer.

The dc magnetization M was measured with a SQUID magnetometer (Quantum Design, MPMS) from 300 K to 1.8 K in magnetic fields $\mu_0 H$ between 0.01 and 7 T in both field-cooled (FC) and zero field cooled (ZFC) conditions. Figure 6(b) shows the temperature dependence of the magnetic susceptibilities ($\chi = M/H$) measured in the field $\mu_0 H = 1 \text{ T}$ along the c axis, and in the ab plane. Above T_N , χ is isotropic, exhibiting the Curie-Weiss behavior above 200 K with the localized moment $\mu_{\text{eff}} = 4.0 \pm 0.2 \mu_B$ [15]. These results suggest that PdCrO_2 constitutes a Heisenberg spin system, consistent with the expectation of the localized spins of the Cr^{3+} ion ($3d^3$, $S = 3/2$). In contrast, below T_N , at which the spins form a 120° structure [15, 18], χ becomes anisotropic with a sudden decrease at T_N ; the value of χ_{ab} becomes larger than that of χ_c . Such anisotropy is similar to the susceptibility of another delafossite CuCrO_2 [7], but is different from a similar layered TL magnet LiCrO_2 with χ_c larger than χ_{ab} [22]. Within the mean field approximation [23], χ should be isotropic even below T_N if the inter-plane spin configuration is ferromagnetic. The observed anisotropy $\chi_{ab} > \chi_c$ is expected if the inter-plane configuration is

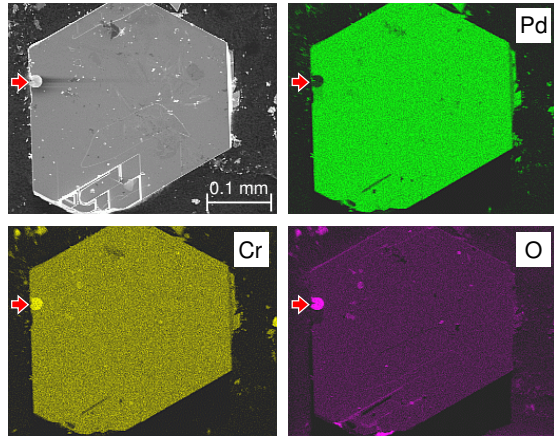


Figure 5: EDX mapping in SEM images of single crystalline PdCrO_2 . The coloring of the images represents the concentration of elements constituting PdCrO_2 : Pd (Green), Cr (Yellow) and O (Purple). The Cr_2O_3 impurity can be seen as a separated phase at the left edge of the crystal (Red arrows).

antiferromagnetic and the spins lie in a plane containing the c axis (the so-called easy-axis type 120° structure). We note that the anisotropy $\chi_{ab} < \chi_c$ for LiCrO_2 is attributed to a 120° structure where the spins lie in the ab plane (the easy-plane type structure) with an antiferromagnetic inter-plane configuration.

4. Conclusion

We have succeeded in growing single crystals of PdCrO_2 by a NaCl flux method. It was confirmed that the obtained crystals are in the delafossite structure with the $R\bar{3}m$ symmetry. The large values of the residual resistivity ratio over 100 and the mean free path in the ab plane as large as $30 \mu\text{m}$ guarantee the high quality of the crystals.

The metallic resistivity with a large anisotropy ($\rho_c/\rho_{ab} > 190$) supports the expectation that the conductivity in PdCrO_2 mainly originates from the Pd layers. The magnetic susceptibility above T_N confirms that PdCrO_2 constitutes a Heisenberg spin system. Moreover, the emergence of the anisotropy at T_N indicates an antiferromagnetic coupling between the layers with the easy-axis type 120° spin structure.

These crystals make possible further investigations of the details of both the actual spin configuration and the Fermi surface topology, as well as searches of other fascinating phenomena related to the frustrated magnetism.

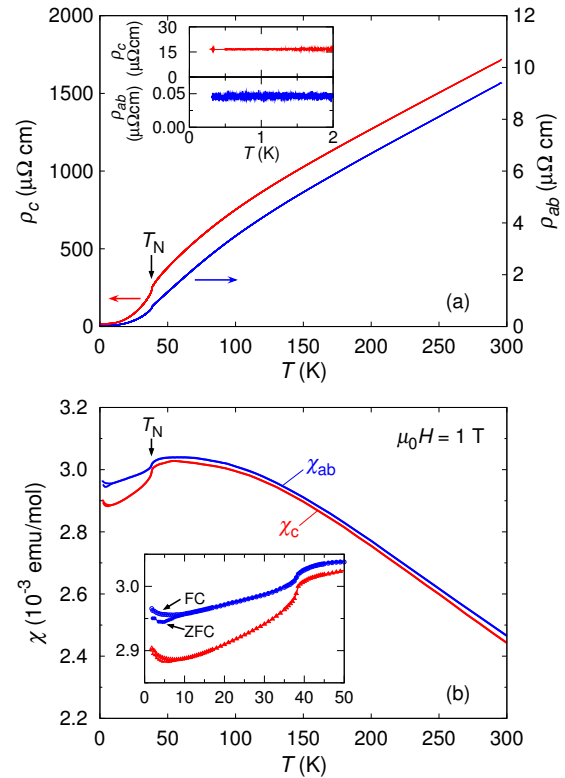


Figure 6: (a) Temperature dependence of the electrical resistivity along the c axis (ρ_c) and in the ab plane (ρ_{ab}). Both ρ_c and ρ_{ab} exhibit clear anomalies at T_N , associated with the antiferromagnetic transition. The inset shows the low temperature behavior of ρ_c and ρ_{ab} . (b) Temperature dependence of the magnetic susceptibilities in the field at 1 T along the c axis (χ_c) and in the ab plane (χ_{ab}). Above T_N , χ_c and χ_{ab} are nearly equal. In contrast, below T_N , χ_c becomes smaller than χ_{ab} . The inset focuses on the behavior near and below T_N . A slight splitting of the ZFC and FC curves appears at temperatures below about 10 K.

Acknowledgements

We would like to thank J. Ishikawa for his assistance of the single crystal growth. We also thank K. Ishida, S. Yonezawa, M. Kriener, D. Peets, Y. Nakai and S. Kitakata for useful discussions and for their experimental assistance. This work was supported by the Grant-in-Aid for the Global COE Program “The Next Generation of Physics, Spun from Universality and Emergence” from the Ministry of Education, Culture, Sports, Science and Technology (MEXT) of Japan and Grants-in-Aids for Scientific Research from the Japan Society for the Promotion of Science (JSPS). H.T. is financially supported as a JSPS research fellow.

References

- [1] G. H. Wannier, Phys. Rev. 79 (1950) 357.
- [2] P. W. Anderson, Mater. Res. Bull. 8 (1973) 153.
- [3] S. Miyashita, H. Shiba, J. Phys. Soc. Jpn. 53 (1984) 1145.
- [4] H. Kawamura, S. Miyashita, J. Phys. Soc. Jpn. 53 (1984) 4138.
- [5] T. Kimura, J. C. Lashley, A. P. Ramirez, Phys. Rev. B 73 (2006) 220301(R).
- [6] S. Seki, Y. Onose, Y. Tokura, Phys. Rev. Lett. 101 (2008) 067204.
- [7] K. Kimura, H. Nakamura, K. Ohgushi, T. Kimura, Phys. Rev. B 78 (2008) 140401(R).
- [8] N. Nagaosa, J. Phys. Soc. Jpn. 75 (2006) 042001.
- [9] A. Wichainchi, P. Dordor, J. P. Doumerc, E. Marquestaut, M. Pouchard, P. Hagenmuller, J. Solid State Chem. 74 (1988) 126.
- [10] E. Wawrzyńska, R. Coldea, E. M. Wheeler, I. I. Mazin, M. D. Johannes, T. Sörge, M. Jansen, R. M. Ibberson, P. G. Radaelli, Phys. Rev. Lett. 99 (2007) 157204.
- [11] H. Takatsu, S. Yonezawa, S. Mouri, S. Nakatsuji, K. Tanaka, Y. Maeno, J. Phys. Soc. Jpn. 76 (2007) 104701.
- [12] H.-J. Noh, J. Jeong, J. J. E.-J. Cho, S. B. Kim, K. Kim, B. I. Min, H. D. Kim, Phys. Rev. Lett. 102 (2009) 256404.
- [13] R. D. Shannon, D. B. Rogers, C. T. Prewitt, Inorg. Chem. 10 (1971) 713.
- [14] M. Itoh, M. Mori, M. Tanaka, H. Takei, Physica B 259-261 (1999) 999.
- [15] H. Takatsu, H. Yoshizawa, S. Yonezawa, Y. Maeno, Phys. Rev. B 79 (2009) 104424.
- [16] H. Takatsu, S. Yonezawa, S. Fujimoto, Y. Maeno (in press).
- [17] K. Momma, F. Izumi, J. Appl. Crystallogr. 41 (2008) 653.
- [18] M. Mekata, T. Sugino, A. Oohara, Y. Oohara, H. Yoshizawa, Physica B 213 (1995) 221.
- [19] J. P. Doumerc, A. Wichainchai, A. Ammar, M. Pouchard, P. Hagenmuller, Mat. Res. Bull. 21 (1986) 745.
- [20] T. Shishidou and T. Oguchi, (Personal communication). Here, the value of k_F is estimated from the band structure calculation.
- [21] The carrier density n is estimated from the ordinary Hall coefficient R_0 with the single band approximation, $R_0 = 1/ne$. It is however difficult to evaluate R_0 of PdCrO_2 because the Hall resistivity in PdCrO_2 contains the anomalous Hall resistivity in addition to the ordinary Hall resistivity. Thus, R_0 of PdCrO_2 is approximated by R_0 of the isostructural nonmagnetic compound PdCoO_2 [16]. This approximation is based on the expectation that one Pd 4d electron per formula unit dominantly contributes to the electric conductivity for both PdCrO_2 and PdCoO_2 . Indeed, the electronic specific heat coefficient, related to the density of states of conduction carriers, is nearly the same between these two oxides.
- [22] H. Kadowaki, H. Takei, K. Motoya, J. Phys. Cond. Matt. 7 (1995) 6869.
- [23] T. Hirone, K. Adachi, J. Phys. Soc. Jpn. 12 (1957) 156.